American Mineralogist, Volume 77, pages 605–616, 1992

Phase equilibria of dikes associated with Proterozoic anorthosite complexes

MIRANDA S. FRAM
Lamont-Doherty Geological Observatory and Department of Geological Sciences, Columbia University, Palisades, New York 10964, U.S.A.

JOHN LONGHI
Lamont-Doherty Geological Observatory of Columbia University, Palisades, New York 10964, U.S.A.

ABSTRACT

We have investigated the petrogenesis of Proterozoic massif anorthosites through experimental phase equilibria studies of two compositions representative of intrusive bodies associated with anorthosite plutons, an anorthositic dike from the Nain Complex and an average high-Al gabbro composition from the Harp Lake Complex. Experiments on both compositions show that liquidus plagioclase becomes distinctly more albitic with increasing pressure. The anorthositic dike composition does not represent a liquid or a simple suspension of plagioclase in liquid because the phase assemblages and mineral compositions produced in the experiments do not match those in thin section. The discrepancy appears to be caused by large-scale heterogeneity in the dike sample, which is also evident in the whole set of anorthositic dike compositions and may be caused by open-system crystallization. The high-Al gabbro composition has plagioclase, orthopyroxene, and high-Ca pyroxene in its liquidus at 11.5 kbar. Orthopyroxene crystals formed at 10–11.5 kbar are similar in major and minor element composition to the most aluminous orthopyroxene megacrysts, and liquidus plagioclase compositions at 10–11.5 kbar overlap the bulk of plagioclase compositions reported for the Harp Lake Complex. These features are consistent with both the orthopyroxene megacrysts and much of the plagioclase crystallizing in lower-crustal or upper-mantle magma chambers from a parental magma similar to the average high-Al gabbro and then intruding upward as mushes or crystal-rich suspensions.

INTRODUCTION

The composition of magmas parental to Proterozoic massif anorthosites has eluded petrologists for a long time. As far back as 1917, N. L. Bowen noted that the fundamental problems of anorthosite genesis are finding a parent magma composition and determining a process by which the high modal proportions of plagioclase in the plutons could be produced. A number of models have been advanced over the years to explain the formation of anorthosites and associated granitic rocks from parental magmas ranging in composition from quartz dioritic (Green, 1969a, 1969b) to anorthositic or hyperfeldspathic (Buddington, 1939; Yoder and Tilley, 1962; Simmons and Hanson, 1978; Wiebe, 1979, 1980; Morse, 1982) to basaltic (Emslie, 1980; Longhi and Ashwal, 1985). There is little agreement on the crystallization conditions as well. Models range from high-pressure fractionation followed by diapiric rise of crystals or liquids (Emslie, 1980; Duchesne et al., 1985; Longhi and Ashwal, 1985) to in situ crystallization (Wiebe, 1979) to fractional crystallization (Green, 1969b). In this study we assess the feasibility of two potential parental magmas, anorthositic and basaltic liquids, by examining the phase equilibria of dikes associated with anorthosite plutons. We combined the results of this experimental study with other observations to assess a model for the genesis of massif anorthosites.

Geology

The Proterozoic massifs are the most voluminous of terrestrial anorthosites, with surface exposures ranging up to 30000 km^2 per complex. In detail, the complexes consist of numerous smaller plutons of variable size and composition (e.g., Emslie, 1980; Morse, 1982). Most massif anorthosites were emplaced between 1.2 and 1.7 b.y. and are associated with anorogenic magmatism or what has been interpreted as failed rifting (Morse, 1982; Emslie, 1985). Syenite, mangerite, and charnockite plutons and Fe-Ti oxide–rich rocks are spatially and temporally associated with many anorthosites. Field and geochemical evidence indicates that the silicic rocks are not comagmatic with the anorthosite plutons, although they are contemporaneous (e.g., Buddington, 1939; Ashwal and Seifert, 1980; Duchesne et al., 1985; Duchesne, 1990). This removes the constraint that anorthosite parent magmas must also be able to produce syenitic or granitic residual liquid through direct fractional crystallization (e.g., Bowen, 1917; Green, 1969b). It is also noteworthy that mafic and ultramafic rocks are not found in great abundance close to any anorthosites.

0003–004X/92/0506–0605$02.00

Petrology

Andesine to labradorite (An_{40}–An_{60}) plagioclase dominates Proterozoic anorthosites, typically forming 70–95% of the rock. The balance consists of olivine or low-Ca pyroxene, with lesser quantities of Fe-Ti oxides and high-Ca pyroxene. The mafic phases typically have values of Mg′ [MgO/(MgO + FeO) in moles] between 0.55 and 0.70, with a maximum near 0.80. Some of the most magnesian pyroxenes are orthopyroxene megacrysts, notable for their large size (10–100 cm) and highly aluminous compositions as evidenced by plagioclase exsolution lamellae. These pyroxenes may be produced by in situ growth from magma oversaturated with pyroxene (Morse, 1975; Dymek and Gromet, 1984) or by crystallization at high pressures followed by transport to shallower levels in the crust (Emslie, 1975; Wiebe, 1986).

Relatively unmetamorphosed anorthosite plutons characteristically have cumulus plagioclase with typically intercumulus mafic minerals. Locally, modal layering with subhedral to euhedral crystals is well developed (Emslie, 1980; Wiebe, 1990), but more commonly the rocks are granular intergrowths of subhedral to anhedral plagioclase. Bent simple or stress-induced multiple twins in some plagioclase crystals (Wiebe, 1978; Longhi and Ashwal, 1985) and foliated margins of some anorthosite plutons (Duchesne et al., 1985) indicate deformation in a partially solid state.

Pressure and temperature conditions of anorthosite emplacement have been quantified by examination of both contact aureoles around anorthosite complexes and the mineralogy of cogenetic plutons. Estimates range from 2 to 4 kbar for gneisses and ironstones around the Nain Complex (Berg, 1977, 1979) to 3 kbar for monzosyenite associated the Laramie anorthosite (Fuhrman et al., 1988) to 5.6–8.7 kbar for monzosyenite in the Wolf River Massif (Anderson, 1980). Pyroxene thermometry in the Nain anorthosite indicates anorthosite crystallization temperatures of 1100–1000 °C at a pressure of 3 kbar (Ranson, 1986). Although the pressure estimates vary from 1.5 to 8.7 kbar, most of the determinations are close to 3 kbar (corresponding to a depth of emplacement of 8–12 km), and crystallization temperatures of the anorthosites are consistent with large layered mafic intrusions. Mineral assemblages in the contact aureoles of anorthosite complexes, in plutons associated with the complexes, and in the anorthosites themselves all suggest that the activity of H_2O in the magmas was very low (e.g., Morse, 1982; Fuhrman et al., 1988; Kolker and Lindsley, 1989).

Parental magmas

Based on Sr, Nd, and Pb isotopic data (e.g., Ashwal and Wooden, 1983; Ashwal et al., 1986), it is generally agreed that the primary magma for anorthosite plutons is ultimately derived from the mantle, although the intermediate values of Mg′ in mafic phases indicate that fractionation of the primary melt occurred before anorthosite production. It is not agreed, however, whether the fractionation generates an evolved basaltic or hyperfeldspathic (anorthositic) parental magma.

Anorthositic magmas, with bulk compositions close to the anorthosite plutons themselves, have been proposed as parental magmas based on field and geochemical data. Perhaps the strongest argument has been the existence of anorthositic dikes in the vicinity of several anorthosite complexes, in particular the Nain Complex, that have been interpreted as representing liquids (Wiebe, 1979, 1980) or plagioclase-liquid suspensions (Wiebe, 1990). REE modeling suggested that anorthositic chill margins on some anorthosites are in equilibrium with cumulate anorthosites and thus consistent with being parental magmas (Simmons and Hanson, 1978). However, Green (1969b), Emslie (1970), and Longhi and Ashwal (1984) note that a major obstacle to an anorthositic parental magma is the difficulty of forming such an aluminous liquid. Morse (1982) proposes that hyperfeldspathic liquids are generated by delayed nucleation of plagioclase in a basaltic magma fractionally crystallizing mafic minerals. Wiebe (1990) suggests that plagioclase content of a basaltic magma could be increased by significant decompression melting of suspended plagioclase.

It has also been proposed that anorthosites are formed directly from an evolved basaltic parental magma. The high proportion of plagioclase in the plutons is generated by mechanical enrichment of plagioclase crystals either at high pressures (e.g., Longhi and Ashwal, 1985; Miller and Weiblen, 1990; Phinney et al., 1988; Bridgwater, 1967) or low pressures (e.g., Emslie, 1980). Many anorthosite complexes include a suite of dikes and small intrusions with basaltic compositions (Emslie, 1980).

Experimental studies of dike phase equilibria

Samples

In order to assess the models involving anorthositic and basaltic parent magmas, we have examined the phase equilibria of two important dike types associated with anorthosites using starting materials representative of each type. Since most anorthosites appear to have crystallized under low H_2O conditions, all of our experiments were conducted under anhydrous conditions and are therefore only applicable to determining the feasibility of anhydrous anorthosite genesis models. The first sample is from an anorthositic dike in the Nain Complex (sample 500B provided by R. Wiebe) (Table 1). The dike is moderately coarse grained with grain sizes ranging from 0.5 to 5 mm and has ortho- to mesocumulus texture. Plagioclase makes up almost 90% of the rock; grains are zoned with An_{50}–An_{55} cores and An_{42}–An_{47} rims. The major mafic phases are anhedral to subhedral inverted pigeonite with coarse augite lamellae along (001) and finer augite lamellae along (100) of the orthopyroxene host, making it similar in appearance to inverted pigeonite found in the main Nain anorthosites by Ranson (1986) and anhedral to subhedral augite with orthopyroxene exsolution lamellae. Some in-

terstitial orthopyroxene, Fe-Ti oxides, quartz, alkali feldspar, and apatite are also present. The complex normal and patchy zoning patterns and large compositional range (maximum An_{55}–An_{35}) in dike plagioclase crystals and the primary hypidiomorphic textures (Wiebe, 1979, 1990) suggest that the crystals have not reequilibrated and annealed, so the plagioclase compositions are primary. This contrasts with the pyroxenes, which are usually unzoned and exsolved, reflecting extensive reequilibration. The petrography of the dikes allows for two types of experimental tests. If the dike represents a liquid, then liquidus experiments should recover the natural plagioclase core compositions. If the dike is instead a suspension of plagioclase in liquid, then the phase assemblage in the natural rock, plagioclase + pigeonite and augite, should be produced in melting experiments, although the Fe-Mg composition of the pyroxene may be different.

The second starting material used in this study is a synthetic glass made to match the average high-alumina gabbro composition from the Harp Lake Complex as reported by Emslie (1980) (Table 1). This composition is taken from a composite of samples from dikes, marginal rocks, and discrete small intrusive bodies. The high-alumina gabbros range in texture from coarse to fairly fine grained to porphyritic. Their mineral content is characterized by plagioclase and olivine or orthopyroxene ± augite. The glass was synthesized from reagent grade oxides and carbonates. After subsolidus decarbonation, the oxide mix was fused several times above liquidus temperature in a Pt crucible that had been presaturated with Fe. The final fusion took place at 1250 °C in a CO-CO_2 atmosphere, controlled to an f_{O_2} of one log unit below QFM. Both starting materials were finely ground in an agate mortar under alcohol, dried overnight at 125 °C, and then stored in a desiccator until used.

Table 1. Electron microprobe analyses of starting compositions

	500B Nain Dike (natural)	HLCA Harp Lake Dike (synthetic)
SiO_2	55.85	50.02
TiO_2	0.52	1.85
Al_2O_3	22.92	17.51
Cr_2O_3	0.01	0.03
FeO	3.50	10.97
MnO	0.06	0.15
MgO	1.40	6.67
CaO	9.55	8.78
Na_2O	4.67	2.93
K_2O	0.90	0.44
P_2O_5	0.16	0.16
Total	99.52	99.50

Experimental methods

Experiments at 1 bar were conducted in a Deltech gas mixing furnace, with f_{O_2} maintained at QFM − 1 in a CO-CO_2 atmosphere. Each experiment consisted of an aliquot of sample powder sintered lightly to a 5-mm diameter Pt loop made of 0.010 or 0.004 in. wire. Although the loops were presaturated by cooking sample at the experimental conditions for 24 h then reusing the same loop for the experiment, Fe loss did occur in some experiments. However, Fe loss was minor in experiments in which the first-crystallizing mafic phase was analyzed (<1% in sample 500B-46, <10% in sample HLCA-6), so the identities and compositions of the mafic phases are considered accurate. Fe loss in the analyzed liquidus experiments was greater (37% in sample 500B-48, 30% in sample HLCA-46). Low gas-flow rates of 0.1 cm/s through the furnace and relatively short experiments minimized alkali loss. No Na loss occurred in the 500B liquidus experiment (500B-48), and after correction for Fe loss, Na loss in the HLCA liquidus experiment (HLCA-46) was 15%. Calculation of liquidus temperatures and plagioclase compositions for the 500B starting composition and the analyzed glass composition from the liquidus experiment (500B-48) using the liquid line of descent program of Weaver and Langmuir (1990) indicates that Fe loss in this experiment could introduce an error of 1 °C in liquidus temperature and 0.005 anorthite units in liquidus plagioclase composition. Similar calculations for HLCA indicate that Fe and Na loss in experiment HLCA-46 could introduce a maximum error of 10 °C in liquidus temperature and 0.030 anorthite units in liquidus plagioclase composition. However, since the cores of plagioclase were analyzed, the error is probably smaller. Thus mineral assemblages, solid phase compositions, and temperatures of phase appearances observed in the 1-bar experiments are thought to be accurate, although the reported liquid compositions for HLCA-46 and 500B-48 are not due to Fe and Na loss. Durations of the experiments varied from 2 to 60 h with short experiments used to define the temperatures of phase appearances and longer experiments in which larger crystals grew used for microprobe analysis (Table 2).

The higher pressure experiments were conducted all in a standard ½-in. Boyd and England (1960) piston cylinder apparatus; 0.0075–0.01 g of sample powder was packed in a graphite capsule and placed in a sintered barium carbonate pressure cell with a crushable alumina filler. The whole assembly was dried overnight in a vacuum oven before beginning an experiment. The cold-piston-in method was used for all the experiments. To minimize problems, nucleating phases near the liquidus of HLCA (the glass starting material) experiments were conducted near the solidus for 6–12 h before raising the temperature to the final value. Durations varied from 4 to 12 h for reconnaissance experiments used to define the temperatures of phase appearances and 12–120 h for experiments to be analyzed by electron microprobe (Table 2). Oxygen fugacity in graphite capsules is at or just below the CCO buffer, which is about QFM − 2.

Temperature and pressure were carefully calibrated and controlled. Several experiments with double junction thermocouples established the thermal gradient across the sample as ~5 °C and the offset between the thermocouple and sample as 20 °C. Temperature was measured and

TABLE 2. Experimental conditions

Experiment	T (°C)	P	t (h)	Phases*
500B-1	1300	1 bar	24	gl + pl
500B-4	1375	1 bar	2	gl
500B-10	1200	1 bar	2	gl + pl
500B-11	1150	1 bar	2	gl + pl
500B-15	1320	10 kbar	11	gl + pl
500B-17	1270	10 kbar	50	gl + pl
500B-19	1220	10 kbar	48	gl + pl + aug
500B-22	1425/1385	10 kbar	24/140.5	gl + pl
500B-23	1395	10 kbar	24	gl + pl?
500B-24	1410	10 kbar	23	gl
500B-25	1460	20 kbar	15	gl
500B-26	1420	20 kbar	15	gl + pl?
500B-27	1370	20 kbar	15	gl + pl
500B-30	1400	20 kbar	24	gl + pl
500B-31	1280	20 kbar	24.7	gl + pl + aug + gnt
500B-32	1325	20 kbar	24	gl + pl + aug
500B-33	1400	30 kbar	24	gl + cor + pl + cpx
500B-42	1130	1 bar	3.25	gl + pl + aug + ilm
500B-43	1370	7 kbar	24	gl + pl
500B-44	1430	27 kbar	86	gl + cor + pl + cpx
500B-45	1450	27 kbar	38	gl + cor + pl
500B-46	1125	1 bar	60	gl + pl + aug + ilm
500B-47	1365	1 bar	6	gl + pl
500B-48	1355	1 bar	10	gl + pl
HLCA-1	1200	1 bar	3	gl + pl + ol
HLCA-2	1100	1 bar	3	gl + pl + ol + hpyx
HLCA-3	1150	1 bar	3	gl + pl + ol
HLCA-6	1175	1 bar	12	gl + pl + ol
HLCA-8	1200	7 kbar	57	gl + pl + lpyx
HLCA-10	1275	10 kbar	24	gl + pl
HLCA-12	1300	10 kbar	4.75	gl
HLCA-13	1250	10 kbar	129	gl + pl + lpyx
HLCA-15	1300	15 kbar	34	gl + hpyx + pl
HLCA-17	1325	15 kbar	63.75	gl
HLCA-21	1200	5 kbar	28.2	gl + pl + lpyx + ol
HLCA-25	1250	13 kbar	34	gl + pl + lpyx + hpyx
HLCA-27	1220/1320	15 kbar	12/30.3	gl + hpyx
HLCA-28	1175/1260	13 kbar	6.3/43.5	gl + pl + hpyx
HLCA-29	1200/1300	13 kbar	6/40.5	gl
HLCA-31	1200/1290	13 kbar	6.5/91.7	gl + aug
HLCA-32	1220/1275	11.5 kbar	6.5/48	gl + pl + hpyx + lpyx
HLCA-38	1210	1 bar	3	gl + pl
HLCA-40	1240	1 bar	3	gl
HLCA-41	1230	1 bar	13	gl + pl
HLCA-43	1250	7 kbar	24	gl + pl
HLCA-44	1175	6 kbar	48	gl + pl + lpyx
HLCA-46	1228	1 bar	48	gl + pl

Note: Experiments with two times listed were conducted at two temperatures; the second is the temperature plotted in Figures 1 and 3.
* Phases: gl = glass, pl = plagioclase, aug = augite, gnt = garnet, cor = corundum, cpx = Ca-Tschermak clinopyroxene, ilm = ilmenite, ol = olivine, lpyx = low-Ca pyroxene, hpyx = high-Ca pyroxene.

controlled with Pt/Pt + 10%Rh thermocouples, and thermocouple emf was not corrected for pressure. Pressure was calibrated by differential thermal analysis of the melting point of Au as reported by Akella and Kennedy (1971). The pressure difference between the applied and the actual pressure is linear between 5 and 30 kbar, ranging from 2 kbar at 5 kbar to 4.5 kbar at 30 kbar. This is very similar in magnitude to the constant 3-kbar correction reported for barium carbonate–chrome oxide cells (Walker and Agee, 1987).

All experiments were done under anhydrous conditions. As a check on the H_2O contents of the experiments, two superliquidus piston cylinder experiments conducted at 10 kbar for 8 and 123 h were examined by FTIR by V. Pan at Arizona State University and found to have less than 0.15 wt% H_2O and negligible CO_2. This is considered to represent the maximum H_2O content of the experiments since these two experiments were conducted during the hottest and most humid part of the year.

After each experiment, the samples were either lightly crushed for examination under transmitted light and large chunks mounted in epoxy for reflected light study, or the whole pressure cell from piston cylinder experiments was mounted directly in epoxy without crushing. Well compacted textures commonly developed in longer experiments, probably because of the slight thermal gradient across the sample (Lesher and Walker, 1988).

Electron microprobe analyses of phases in selected experiments were performed on the Cameca Camebax/Micro wavelength dispersive system at Lamont-Doherty. An accelerating voltage of 15 kV and sample currents of 5 nA for K and Na and 25 nA for Si, Ti, Al, Fe, Mg, Mn,

TABLE 3. Electron microprobe analyses of experimental products—500B

Expt.	Phase*	SiO_2	TiO_2	Al_2O_3	Cr_2O_3	FeO	MnO	MgO	CaO	Na_2O	K_2O	P_2O_5	Sum	An or Mg'
19	glass(5)	55.01	1.38	14.74	0.01	9.56	0.17	3.52	8.48	3.76	1.66	0.62	98.91	
	plag(11)	56.42	0.04	27.63		0.34		0.05	10.24	4.93	0.51		100.19	0.518
	aug(10)	52.30	0.77	3.26	0.06	8.70	0.21	14.97	20.24	0.53			101.04	0.754
		(0.68)	(0.17)	(0.55)	(0.01)	(0.33)	(0.02)	(0.42)	(0.46)	(0.08)				
22	glass(5)	55.71	0.39	22.73	0.00	3.44	0.07	1.53	9.51	4.66	0.97	0.22	99.24	
	plag(11)	52.63	0.02	31.02		0.15		0.06	13.47	3.64	0.15		101.15	0.665
30	glass(5)	55.59	0.58	22.57	0.02	3.47	0.06	1.44	9.32	4.52	0.99	0.16	98.72	
	plag(10)	55.41	0.03	28.54		0.21		0.05	10.95	4.67	0.30		100.19	0.554
32	glass(5)	55.67	1.05	18.93	0.01	6.39	0.10	2.40	9.05	4.07	1.41	0.27	99.35	
	plag(11)	56.68	0.04	27.91		0.25		0.05	10.04	5.09	0.49		100.58	0.506
	aug(5)	48.57	0.52	15.75	0.08	6.08	0.13	9.44	19.31	1.94			101.82	0.734
		(0.59)	(0.06)	(0.30)	(0.02)	(0.14)	(0.02)	(0.13)	(0.17)	(0.13)				
43	glass(6)	55.31	0.50	23.09	0.01	3.43	0.05	1.45	9.51	4.80	0.92	0.24	99.31	
	plag(9)	50.84	0.04	32.19		0.14		0.05	14.25	3.41	0.13		101.03	0.693
44	glass(5)	57.94	0.60	22.24	0.00	3.72	0.07	1.25	9.08	4.59	1.10	0.44	101.04	
	plag(5)	57.13	0.02	27.66		0.14		0.04	8.97	5.75	0.35		100.06	0.453
	cpx(5)	44.51	0.46	25.76	0.01	3.48	0.08	5.05	17.53	3.12			100.00	0.721
		(0.74)	(0.07)	(1.61)	(0.01)	(0.31)	(0.02)	(0.74)	(0.37)	(0.15)				
46	glass(7)	57.00	1.42	14.41	0.01	9.90	0.17	3.41	7.30	3.69	2.08	1.01	100.39	
	plag(6)	56.94	0.04	28.38		0.33		0.02	10.20	5.28	0.49		101.68	0.501
	aug(8)	50.65	0.39	1.55	0.03	14.22	0.34	12.23	20.86	0.28			100.55	0.604
		(0.85)	(0.09)	(0.26)	(0.04)	(1.68)	(0.04)	(1.74)	(1.30)	(0.02)				
	ilm	0.02	58.63	0.39	0.11	34.35	0.42	6.52	0.08	0.00			100.52	
48	glass(6)	57.10	0.71	22.85	0.01	2.19	0.08	1.40	9.07	4.76	0.89	0.16	99.22	
	plag(10)	49.25	0.09	33.04		0.04		0.11	15.36	2.60	0.08		100.58	0.761

Note: An [Ca/(Ca + Na + K) in atomic units] is given for plagioclase; Mg' [MgO/(MgO + FeO) in moles] is given for pyroxene.
* Phases: plag = plagioclase, aug = augite, cpx = Ca-Tschermak clinopyroxene, ilm = ilmenite. Numbers in parentheses next to phase name refer to the number of electron microprobe analyses averaged together. Standard deviations are reported for pyroxene analyses only (see text).

Ca, P, and Cr were used. To minimize alkali loss from glasses, a 5-μm-square raster was used. All other analyses were done with a point beam. For glass analyses, Ca, Mg, Si, and Al were calibrated on a glass standard and all the other elements on minerals or oxides; for mineral analyses, all elements were calibrated on minerals or oxides.

The data reported in Tables 3 and 4 represent averages of five to seven analyses for glasses and five to 11 analyses for mineral phases. Standard deviations for Si, Al, Fe, Mg, Ca, and Na on averages of glass analyses are less than 5% of the amount present. For averages of plagioclase analyses, the standard deviations are generally less than 5% and always less than 10% of the amount present for Si, Al, Ca, and Na. This corresponds to a standard deviation of average anorthite contents of less than 0.018 in most cases and less than 0.029 in all cases. Averaged pyroxene analyses show greater dispersion, especially for Al, and standard deviations are reported in Tables 3 and 4.

EXPERIMENTAL RESULTS

Sample 500B

Experiments on sample 500B yielded the phase diagram shown in Figure 1. As expected from such a feldspar-rich composition, plagioclase is the liquidus phase to >20 kbar. The liquidus temperatures are rather high, ranging from 1365 °C at 1 atm to 1420 °C at 20 kbar. This experimentally determined liquidus is approximately 100 °C higher than the one calculated by Wiebe (1990) for the same composition using the Silmin program of Ghiorso (1985). The phase following plagioclase at all

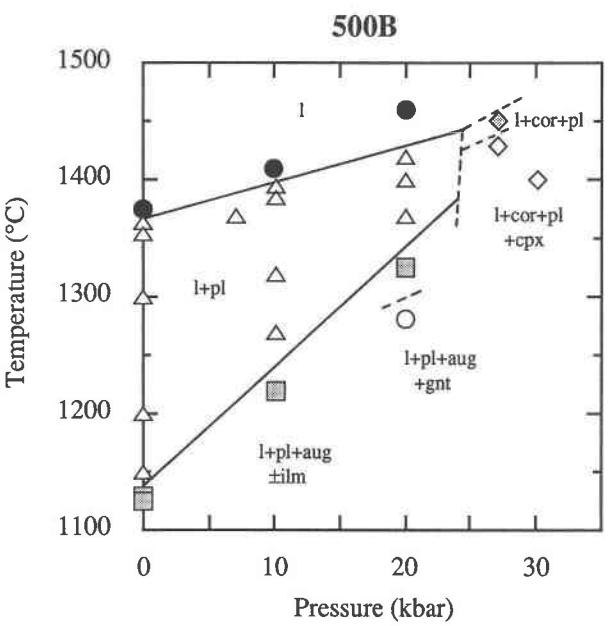

Fig. 1. Experimentally determined pressure-temperature diagram for 500B. Lines separate fields for all liquid (solid circles), liquid + plagioclase (open triangles), liquid + plagioclase + augite ± ilmenite (shaded squares), liquid + plagioclase + augite + garnet (open circle), liquid + corundum + plagioclase + pyroxene (open diamonds), and liquid + corundum + plagioclase (shaded diamond). Boundaries are dashed where less well constrained.

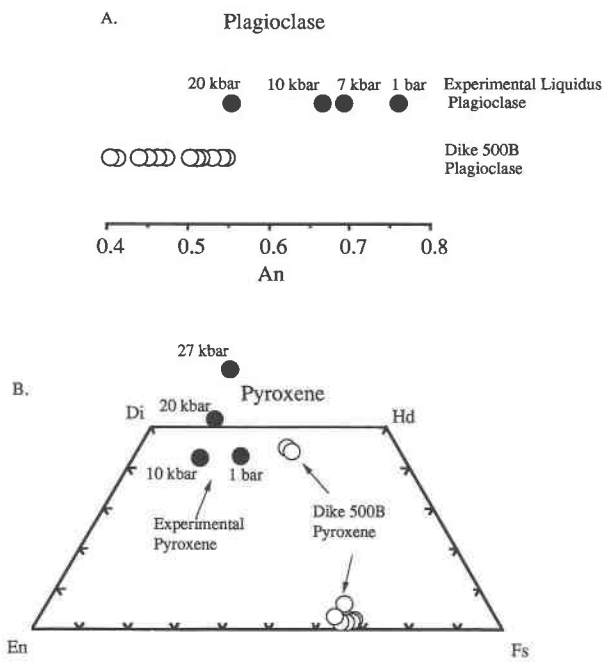

Fig. 2. Comparison of plagioclase and pyroxene compositions produced in the 500B experiments with the phase compositions in thin sections of 500B. (**A**) Anorthite content of experimental liquidus plagioclase (solid circles with pressures of the experiments) and of plagioclase in 500B analyzed by electron microprobe (open circles). (**B**) Pyroxene compositions on an En ($MgSiO_3$)–Fs ($FeSiO_3$)–Di ($CaMgSi_2O_6$)–Hd ($CaFeSi_2O_6$) quadrilateral. Pyroxenes produced in experiments (solid circles with pressures of the experiments) are augite at low pressures and Ca-Tschermak clinopyroxene at higher pressure and are distinct in composition from the augite and inverted pigeonite hosts in 500B analyzed by microprobe (open circles).

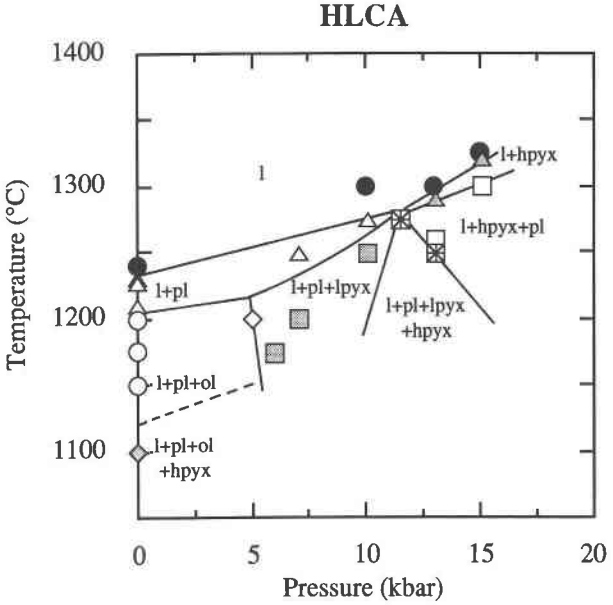

Fig. 3. Experimentally determined pressure-temperature diagram for HLCA. Lines separate fields for all liquid (solid circles), liquid + plagioclase (open triangles), liquid + plagioclase + olivine (open circles), liquid + plagioclase + olivine + high-Ca pyroxene (shaded diamond), liquid + plagioclase + low-Ca pyroxene + olivine (open diamond), liquid + plagioclase + low-Ca pyroxene (shaded squares), liquid + high-Ca pyroxene (shaded triangles), liquid + plagioclase + low-Ca pyroxene + high-Ca pyroxene (crossed squares), and liquid + high-Ca pyroxene + plagioclase (open squares). Boundaries are dashed where less well constrained. Note that the liquidus phase changes from plagioclase at low pressures to plagioclase + high- and low-Ca pyroxene at 11.5 kbar to high-Ca pyroxene at higher pressures.

pressures is augite, appearing 200 °C below the liquidus after ~60% crystallization at 1 bar and about 75 °C below after ~45% crystallization at 20 kbar. At 20 kbar, plagioclase and augite are followed by garnet. Based on the texture in sample 500B-45 (27 kbar, 1450 °C) corundum is the liquidus phase at 27 kbar. It is followed by plagioclase and then a Ca-Tschermak pyroxene.

The composition of the liquidus plagioclase varies from An_{76} at 1 bar to An_{55} at 20 kbar (Fig. 2), although the liquid composition remains nearly constant (Table 3), suggesting a large pressure effect on the plagioclase partition coefficients. Earlier experimental studies on quartz diorite, gabbroic anorthosite, and high-alumina basalt liquids also showed a large pressure dependence for the liquidus plagioclase composition (Green, 1969b). The composition of the plagioclase when augite first appears changes very little, shifting from An_{50} at 1 bar to An_{51} at 20 kbar. A possible explanation for this seemingly different behavior is that both pressure and liquid composition have a major effect on the plagioclase composition. Along the liquidus, compositional variation in the liquid is minimal so the effect of pressure is dominant, whereas the liquids at the first appearance of augite vary considerably in composition (Table 3), with total plagioclase component and anorthite in the normative plagioclase increasing substantially with pressure. As pressure increases, the interval of plagioclase-only crystallization before the appearance of augite becomes narrower. In addition, there is less compositional difference between the crystallizing plagioclase and the liquid's normative plagioclase (distribution coefficient closer to 1), which leads to less change in An/Ab per unit of crystallization. Consequently, the liquids at augite saturation have higher An/Ab with increasing pressure, which counterbalances the trend toward more albitic plagioclase with increasing pressure.

Sample HLCA

Experiments on sample HLCA yielded the pressure-temperature phase diagram shown in Figure 3. From 1 bar to just over 10 kbar, plagioclase is the liquidus phase, followed by olivine at low pressures (≤5 kbar) and orthopyroxene at higher pressures (5–10 kbar). Nearer to the solidus, pigeonite with 4 wt% CaO replaces orthopyroxene. At about 11.5 kbar, HLCA is multiply saturated with plagioclase, orthopyroxene, and high-Ca py-

Table 4. Electron microprobe analyses of experimental products—HLCA

Expt.	Phase*	SiO_2	TiO_2	Al_2O_3	Cr_2O_3	FeO	MnO	MgO	CaO	Na_2O	K_2O	P_2O_5	Sum	An or Mg'
6	glass(7)	50.60	1.95	16.11	0.04	12.69	0.20	6.80	8.51	3.09	0.48	0.18	100.65	
	plag(5)	50.82	0.14	30.87		1.26		0.46	14.15	3.17	0.11		100.98	0.707
	oliv(7)	38.77	0.05	0.15	0.05	21.28	0.26	41.07	0.27	0.01			101.91	0.775
8	glass(5)	49.40	2.46	15.73	0.03	12.80	0.21	6.52	8.40	3.31	0.60	0.20	99.65	
	plag(8)	53.50	0.11	29.86	0.01	0.64	0.02	0.22	12.67	4.02	0.16		101.20	0.629
	lpyx(7)	53.21	0.64	4.11	0.17	14.92	0.22	26.03	2.18	0.16			101.67	0.757
		(0.35)	(0.06)	(0.72)	(0.08)	(0.27)	(0.02)	(0.52)	(0.13)	(0.18)				
10	glass(5)	49.99	1.91	17.41	0.02	11.05	0.16	6.68	8.71	2.92	0.46	0.13	99.45	
	plag(9)	54.14	0.06	29.61		0.44		0.16	12.06	4.24	0.16		100.87	0.605
13	glass(5)	49.14	2.16	16.99	0.02	12.01	0.16	6.37	8.73	3.27	0.47	0.17	99.50	0.600
	plag(11)	54.36	0.07	29.25		0.45		0.15	11.97	4.29	0.19		100.74	0.765
	lpyx(10)	52.15	0.43	6.57	0.29	13.94	0.21	25.41	2.29	0.11			101.39	
		(0.44)	(0.06)	(0.32)	(0.02)	(0.44)	(0.03)	(0.63)	(0.13)	(0.03)				
15	glass(5)	49.99	2.08	18.47	0.01	11.26	0.14	5.58	8.03	3.40	0.52	0.18	99.65	
	plag(10)	56.85	0.07	27.77		0.47		0.13	10.17	5.03	0.26		100.78	0.519
	hpyx(10)	49.71	0.65	11.40	0.17	11.24	0.21	15.77	11.29	1.07			101.50	0.714
		(0.51)	(0.07)	(0.94)	(0.04)	(0.53)	(0.02)	(0.81)	(0.90)	(0.07)				
21	glass(5)	50.58	2.07	15.78	0.04	12.56	0.18	6.98	8.51	3.13	0.52	0.24	100.59	
	plag(7)	52.13	0.09	30.25		0.61		0.22	12.79	3.92	0.10		100.10	0.639
	oliv(4)	38.45	0.09	0.11	0.06	22.95	0.25	39.87	0.32	0.02			102.13	0.756
	lpyx(8)	52.86	0.56	3.45	0.21	14.12	0.27	26.24	2.66	0.10			100.48	0.768
		(1.14)	(0.06)	(0.46)	(0.04)	(0.22)	(0.03)	(0.65)	(0.40)	(0.04)				
27	glass(6)	50.44	1.95	17.82	0.02	10.74	0.16	5.82	8.55	3.37	0.49	0.18	99.53	
	hpyx(10)	48.72	0.77	11.66	0.22	9.81	0.19	15.19	12.92	1.15			100.65	0.734
		(0.50)	(0.24)	(0.65)	(0.04)	(0.98)	(0.03)	(0.74)	(1.14)	(0.17)				
28	glass(6)	50.59	2.18	17.98	0.03	11.63	0.13	5.81	8.23	3.14	0.56	0.22	100.51	
	plag(3)	55.73	0.03	28.67		0.55		0.15	10.68	5.01	0.24		101.06	0.533
	hpyx(7)	49.04	1.14	9.57	0.15	13.02	0.24	17.69	9.47	0.75			101.08	0.708
		(0.29)	(0.32)	(0.75)	(0.05)	(0.92)	(0.03)	(0.29)	(0.79)	(0.12)				
31	glass(6)	49.69	1.98	18.05	0.02	11.13	0.14	5.92	8.38	3.34	0.47	0.18	99.29	
	hpyx(8)	49.42	0.72	11.21	0.27	10.36	0.22	16.23	11.81	0.98			101.28	0.736
		(0.52)	(0.12)	(1.18)	(0.07)	(0.50)	(0.02)	(0.97)	(0.90)	(0.17)				
32	glass(6)	50.21	1.97	17.48	0.02	11.42	0.15	6.28	8.65	3.14	0.49	0.16	99.98	
	plag(8)	53.06	0.08	29.59		0.50		0.15	11.17	5.12	0.20		99.86	0.540
	hpyx(9)	50.01	0.59	7.84	0.29	12.00	0.23	19.71	8.80	0.60			100.06	0.746
		(0.91)	(0.09)	(0.97)	(0.11)	(0.88)	(0.03)	(0.87)	(1.21)	(0.11)				
	lpyx(10)	51.25	0.37	7.99	0.37	13.28	0.19	25.35	2.30	0.16			101.29	0.773
		(0.50)	(0.04)	(0.78)	(0.04)	(0.19)	(0.03)	(0.34)	(0.19)	(0.03)				
43	glass(8)	50.41	1.87	17.26	0.05	11.12	0.15	6.73	8.65	3.12	0.49	0.16	100.01	
	plag(7)	52.96	0.05	29.70		0.62		0.28	12.48	4.10	0.15		100.33	0.622
46	glass(7)	51.12	1.91	18.20	0.04	7.67	0.18	7.37	9.02	2.56	0.34	0.44	98.85	
	plag(9)	49.20	0.10	32.63		0.40		0.21	15.45	2.68	0.05		100.70	0.759

Note: An [Ca/(Ca + Na + K) in atomic units] is given for plagioclase; Mg' [MgO/(MgO + FeO) in moles] is given for olivine and pyroxene.

* Phases: plag = plagioclase, oliv = olivine, lpyx = low-Ca pyroxene, hpyx = high-Ca pyroxene. Numbers in parentheses after phase name are the number of microprobe analyses averaged together. Standard deviations are reported for pyroxene analyses only (see text).

roxene on the liquidus. A similar composition from a chill margin on the Michikamau anorthosite was also multiply saturated at ~12 kbar (Emslie and Lindsley, 1968). Above this point, aluminous augite is the liquidus phase. At 15 kbar, high-Ca pyroxene is followed by plagioclase then orthopyroxene with falling temperature.

As in the experiments with composition 500B, the compositions of the phases are sensitive to pressure. Liquidus plagioclase varies from An_{76} at 1 bar to An_{60} at 10 kbar (Fig. 4). The compositions of orthopyroxene and high-Ca pyroxene from HLCA experiments and pyroxenes from experiments with 500B vary with pressure, although the substitutions that occur appear to be different. With increasing pressure CaO, Na_2O, and Al_2O_3 rise while MgO, FeO, and SiO_2 fall in liquidus high-Ca pyroxene from HLCA experiments (Fig. 5; Table 4, samples HLCA-32, HLCA-27, and HLCA-31). Almost all of the change can be accounted for by increasing jadeite and Ca-Tschermak components at the expense of diopside-hedenbergite and enstatite-ferrosilite components. Since pyroxene is not a liquidus phase in 500B, pyroxene compositions may be affected by variation in liquid composition as well as pressure. However, similarity between the apparent exchange reactions in 500B pyroxenes and HLCA liquidus high-Ca pyroxenes with increasing pressure suggests the changes in 500B pyroxene compositions are dominantly pressure induced. Like HLCA high-Ca pyroxene, 500B pyroxenes appear to exchange diopside-hedenbergite and enstatite-ferrosilite components for jadeite and Ca-Tschermak components as pressure increases. CaO does not rise (Fig. 5) because low-pressure 500B pyroxenes are mainly diopside-hedenbergite (Fig. 2B), so little exchange of enstatite-ferrosilite for Ca-Tschermak takes place. In the orthopyroxenes however, as pressure and Al_2O_3 increase, CaO rises only slightly and Na_2O remains essentially constant. Since one orthopyroxene is on the liqui-

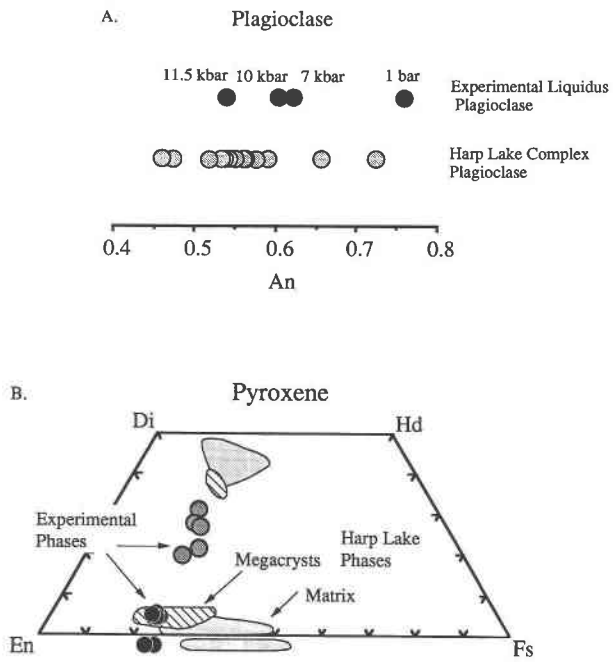

Fig. 4. Comparison of plagioclase and pyroxene compositions produced in the HLCA experiments with the phase compositions in the Harp Lake Complex. (A) Anorthite content of experimental liquidus plagioclase (solid circles with pressures of the experiments) and of plagioclase in the Harp Lake Complex (Emslie, 1980; shaded circles). (B) Pyroxene and olivine compositions on an En ($MgSiO_3$)–Fs ($FeSiO_3$)–Di ($CaMgSi_2O_6$)–Hd ($CaFeSi_2O_6$) quadrilateral. Olivine compositions are plotted below the En-Fs join. Olivine and orthopyroxene produced in the experiments (solid circles), experimental high-Ca pyroxenes (shaded circles), matrix olivine, orthopyroxene, and augite in Harp Lake (Emslie, 1980; light shaded fields), and bulk orthopyroxene megacryst compositions in Harp Lake (Emslie, 1975, 1980; striped field) are plotted.

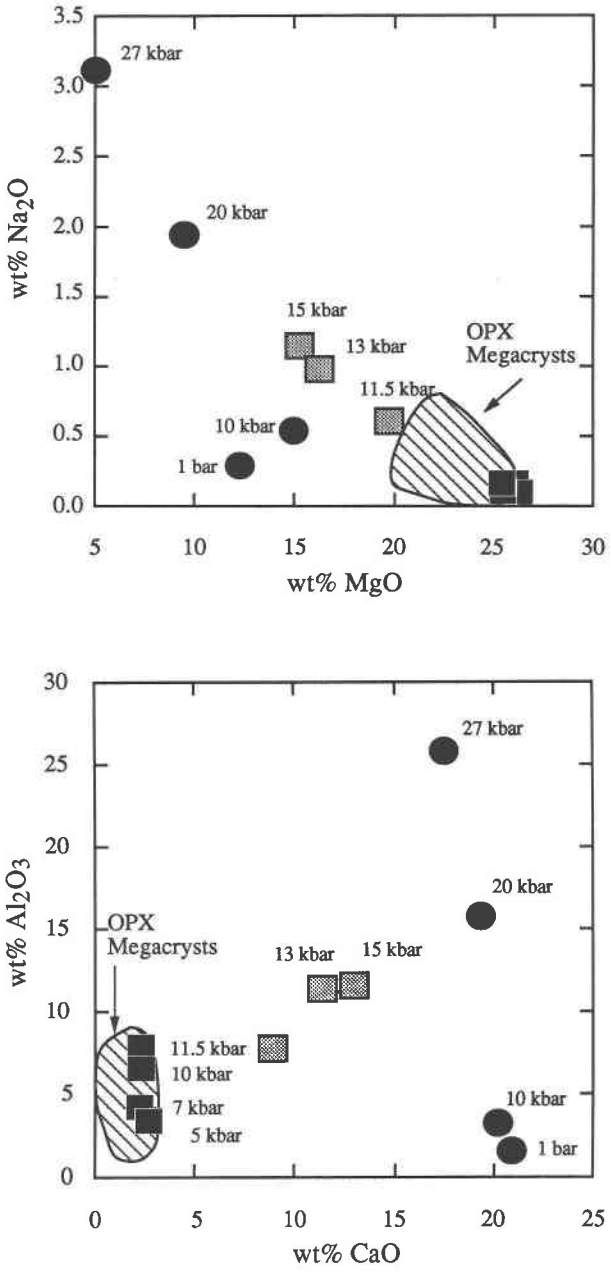

Fig. 5. MgO, Na_2O, CaO, and Al_2O_3 contents of experimental pyroxene and bulk compositions of orthopyroxene megacrysts (striped field; Emslie, 1975, 1980; Dymek and Gromet, 1984; Wiebe, 1986). Sample 500B pyroxene (solid circles), HLCA orthopyroxene (solid squares), HLCA high-Ca pyroxene (shaded squares) are plotted with experimental pressure indicated.

dus (HLCA-32) and three are below (HLCA-6, HLCA-8, HLCA-13), the liquid compositions are not identical, although they are close enough to allow qualitative comparisons among the orthopyroxenes, which show that the substitution to increase Al_2O_3 in orthopyroxene is different than in high-Ca pyroxene. Jadeite and Ca-Tschermak substitution in orthopyroxene do not appear to be very pressure dependent in the range of 5–12 kbar. Al substitution appears to be taking place as an Mg-Tschermak component.

Discussion

Composition 500B

The compositions of the phases produced in the experiments can be compared to the compositions of plagioclase and mafic minerals in the dikes and in the associated anorthosite plutons. Figure 2 shows the compositions of plagioclase and pyroxene from experiments on 500B and microprobe analysis of these phases in samples of the dike. The phases in the dike are very similar to those in the coarse-grained leuconorite anorthosite plutons with which it is associated (Wiebe, 1979). Because the complex zoning patterns and textures of natural 500B plagioclase are primary (Wiebe, 1979, 1990) the compositions must not have been extensively modified by reequilibration. Since the composition of the liq-

uidus plagioclase in the 500B experiments in the range of 1 bar to 7 kbar (An_{76}–An_{69}) is more anorthitic than plagioclase cores (An_{50}–An_{55}) in 500B which crystallized at ~3 kbar (Fig. 2A), 500B has at least accumulated plagioclase. The natural plagioclase does overlap with experimental plagioclase at augite saturation (An_{50}–An_{51}). Wiebe (1990) suggested that 500B might be a solidified suspension of ~30% plagioclase in liquid, in which case the phase assemblage in the sample should still be recovered in the experiments. Mass-balance calculations indicate that the temperature of a 30% suspension would be ~1290 °C at 3 kbar, which is probably excessive for a magma with an intermediate value of Mg′. Furthermore, although the natural pyroxenes in thin sections of 500B are inverted pigeonite and augite, the only pyroxene observed in the experiments was augite with a higher value of Mg′ than either of the natural pyroxenes (Fig. 2B).

An explanation for these discrepancies is that 500B is heterogeneous on a scale larger than a hand sample. Projection of 500B bulk composition from plagioclase is about equidistant from augite and low-Ca pyroxene (Fig. 6), suggesting that the mafic component should be equally split between the two. In addition the value of Mg′ for 500B (0.42) is the same as for natural augite but not as for the low-Ca pyroxene, indicating that augite is more important in the rock composition than our thin section modes indicate. This heterogeneous distribution of mafic phases is also evident on the larger scale of the whole group of anorthositic dikes. Projected from plagioclase, compositions of anorthositic dikes from the Nain Complex (Wiebe, 1990) scatter across the olivine-plagioclase, augite-plagioclase, and low-Ca pyroxene–plagioclase fields rather than grouping along any cotectics (Fig. 6). Since low-Ca pyroxene is the dominant pyroxene, one would expect the majority of the dikes to project into the low-Ca pyroxene–plagioclase field if they represented plagioclase-liquid suspensions feeding the anorthosites. The random scatter suggested that the dike compositions have been affected by accumulation of mafic phases in addition to plagioclase.

Based on the crystallization of more anorthitic plagioclase and more magnesian pyroxenes in the experiments than in the natural sample (Fig. 2), 500B does not represent a liquid composition. Moreover, the analyses of anorthositic dikes are not simply those of suspensions of plagioclase in liquid; there is evidence for accumulation of mafic phases as well (Fig. 6). One mechanism for accomplishing this is open-system crystallization. A suspension with some crystals in liquid moves out into a dike, cooling and crystallizing as it travels. The suspended and newly formed crystals plate out on the walls of the dike, and the remainder of the liquid leaves the system. Liquid might continue to migrate even after the load of suspended crystals comes to rest. Hand specimens of the resulting dike are neither pure liquids nor simple suspensions, and their bulk compositions are not similar to those from which the minerals crystallized. In light of these experimental results, we interpret 500B as an apophysis of the pluton that crystallized under open-system conditions rather than a feeder dike.

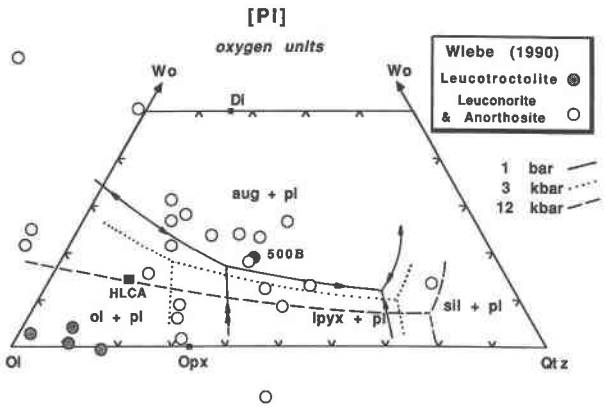

Fig. 6. Projection from plagioclase onto the olivine-wollastonite-silica surface; 1-bar and 12-kbar phase boundaries are estimated based on results of 500B and HLCA experiments; 3-kbar boundaries are interpolated. Liquidus field labels refer to 1-bar boundaries. Compositions of leucotroctolite (shaded circles) and leuconorite and anorthosite (open circles) dikes from the Nain Complex (Wiebe, 1990) and the compositions of 500B (solid circle) and HLCA (solid square) are plotted.

Composition HLCA

The mafic phases produced in the HLCA experiments match the compositions of mafic phases in the Harp Lake Complex (Emslie, 1980), including the orthopyroxene megacrysts, rather well. Low-Ca pyroxene and olivine produced in the experiments lie close to the magnesian end of matrix phases in the Harp Lake Complex and overlap orthopyroxene megacryst compositions (Fig. 4B). Experiments at 3 kbar would provide the most appropriate comparison for matrix phase compositions, but these cannot be done with precision in a piston cylinder. Comparison of experimental pyroxene with bulk analyses of megacrysts from the Harp Lake (Emslie, 1975, 1980), Nain (Wiebe, 1986), St.-Urbain (Dymek and Gromet, 1984), and other (Emslie, 1980) anorthosites shows that experimental orthopyroxenes resemble the megacrysts in terms of major and minor elements (Figs. 5, 6). This overlap indicates that it is possible to form the megacrysts by high-pressure crystallization of a basaltic magma as suggested by Emslie (1975) and Wiebe (1986), although it does not rule out an in situ model of formation (Morse, 1975; Dymek and Gromet, 1984).

Liquidus plagioclase compositions from 1 bar to 11.5 kbar (An_{76}–An_{54}) overlap the range of plagioclase compositions (An_{74}–An_{45}) in anorthositic rocks from the Harp Lake Complex (Emslie, 1980) (Fig. 4A). However, there is a clustering of Harp Lake plagioclase compositions between An_{52} and An_{60} that is similar to the range observed in experimental liquidus plagioclase between 11.5 and 10 kbar (An_{60}–An_{54}). This relationship is consistent with the hypothesis that much of the plagioclase crystallized from a liquid similar to HLCA at the same pressure as the most

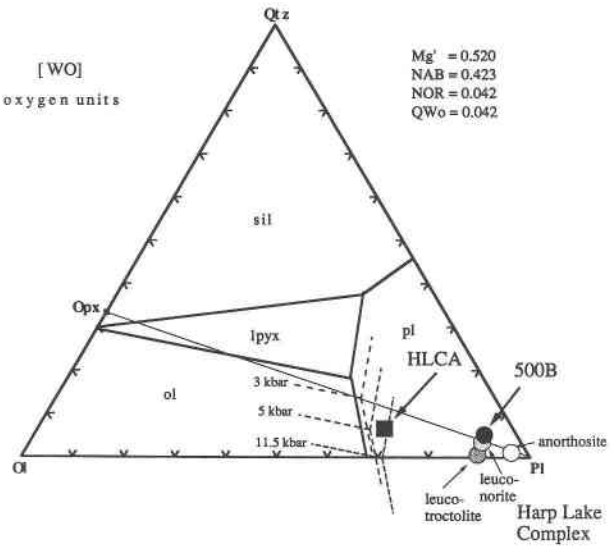

Fig. 7. Projection from wollastonite on the olivine-plagioclase-silica plane; 1-bar phase boundaries were calculated by the method of Longhi (1991), where NAB and NOR are the albite and orthoclose fractions of the molecular normative feldspar and QWo is the Quaternary wollastonite component. The 5-kbar boundaries were positioned by projecting the liquid from HLCA-21, 3-kbar boundaries interpolated between the 1-bar calculated boundaries and the 5-kbar position, and 11.5-kbar boundary positions based on HLCA-32. Bulk compositions of HLCA (solid square) and 500B (solid circle) project into the plagioclase field at low pressure, and 500B resembles the bulk composition of anorthosite (open circle), leuconorite (light shaded circle), and leucotroctolite (dark shaded circle) from the Harp Lake Complex (Emslie, 1980).

aluminous orthopyroxene megacrysts and that both plagioclase and megacrysts were then transported in mushes or suspensions to present locations in the upper crust. More calcic Harp Lake plagioclase (including reversely zoned rims) may then represent crystallization from the matrix liquid at the site of intrusion. However, since mass balance also exerts strong control on solid composition in mixtures of solid and liquid, a variety of zoning profiles could be generated locally depending on the relative volumes of liquid and plagioclase.

The experiments on HLCA indicate that the phase boundaries move significantly as a function of pressure between 1 bar and 15 kbar. Projecting from the wollastonite component onto the olivine-silica-plagioclase plane allows the fields of olivine, orthopyroxene, and plagioclase to be visible. The 1-bar phase boundaries in the projection shown in Figure 7 are calculated by the method of Longhi and Pan (1988) and Longhi (1991), which accounts for the movement of the phase boundaries with a changing value of Mg′ and alkali components of the liquid. The diagram shows the phase boundaries on a plane cut through the wollastonite-quartz-plagioclase-olivine tetrahedron at the approximate wollastonite content of the HLCA liquid. Experiment HLCA-21 (5 kbar, 1200 °C) locates the olivine–low-Ca pyroxene–plagioclase point at 5 kbar. The positions of the low-Ca pyroxene–plagioclase boundary at higher pressures are constrained by projecting glass compositions from multiply saturated experiments (Table 4). The positions of the boundaries at 3 kbar, the pressure of anorthosite emplacement, are estimated. The projected points of HLCA and 500B lie within the plagioclase field at pressures less than 11.5 kbar, and the 500B bulk composition is very similar to the average compositions of anorthositic rocks in the Harp Lake Complex (Fig. 7). As is evident in Figures 1 and 3, liquids with these compositions crystallize plagioclase first at these pressures. The volume of plagioclase crystallized by the two compositions at various pressures can be estimated from the modes in the experimental charges or directly from Figure 7 since the O units used in the projection closely approximate volume proportions. About 12% plagioclase crystallizes from HLCA at 3 kbar before saturation with a mafic phase is reached, whereas about 60% plagioclase crystallizes from 500B at that pressure.

Since decompression of HLCA from 11.5 kbar, where it is multiply saturated with plagioclase and pyroxenes, to 3 kbar only generates ~10% excess plagioclase, a large volume of magma must be processed if the high proportion of plagioclase is generated by decompression alone. Given 3-kbar proportions of plagioclase and mafic minerals of 70:30, closed-system crystallization of HLCA would produce about 73% plagioclase. To produce a rock with 90% plagioclase, only 6% of the residual cotectic liquid could remain with the 10% excess plagioclase. Thus approximately 80% or more of the parental magma must have crystallized somewhere else, either as cumulates or as extrusives. The absence of large coeval mafic plutons or extensive volcanics suggests that most of the missing volume of magma is not in the upper crust. Thus the mechanical enrichment of plagioclase is more likely to have taken place in a higher pressure staging area rather than at the final shallow level of the anorthosite plutons. This pressure for the Harp Lake Complex is presumably 10–12 kbar where there is a close match between experimental and natural phase compositions.

The density relationships among the phases in HLCA-32 (11.5 kbar, 1275 °C) indicate that the plagioclase will float, but the pyroxenes sink. Using the formula of Bottinga and Weill (1970), the partial molar volume data of Mo et al. (1982), and silicate liquid compressibility from Agee and Walker (1988), the density of the HLCA-32 liquid is 2.73 g/cm³. The density of An_{54} plagioclase is only 2.68 g/cm³, corrected for thermal expansion (Skinner, 1966) and compressibility (Birch, 1966), so it should float. However, in the experimental charge, all of the crystals (plagioclase and pyroxenes) are less than 50 μm and compacted on the bottom of the charge. Since the Stokes settling (or rising) velocity depends on size, the absence of plagioclase flotation may be due to insufficient time for such small crystals to float. In addition, the competing effect of compaction in the thermal gradient helps pin the crystals to the bottom of the sample. In experiment HLCA-43 (7 kbar, 1245 °C), which has a similar density contrast between liquid (2.76 g/cm³) and plagio-

clase (2.68 g/cm^3), plagioclase crystals 50–100 μm are floating in the center of the sample, whereas smaller ones are lying on the bottom.

Anorthosite formation

In light of the petrologic and geologic features of Proterozoic massif anorthosites and the results of the experiments on HLCA, we can devise a model for the petrogenesis of anorthosite plutons from a parent magma similar to HLCA. Crystallization of mafic minerals from a primitive magma in a lower crust or upper mantle at 11.5 kbar (~35 km) produces an evolved magma with an intermediate value of Mg′ similar in composition to HLCA, which is saturated with plagioclase, orthopyroxene, and high-Ca pyroxene. A floating mat of intermediate composition plagioclase crystals with a few entrained pyroxene (the megacrysts) accumulates at the top of the chamber. Wiebe (1990) has suggested that repeated intrusion of hot, primitive magma might partially melt the suspended crystals and enrich the matrix liquid in the plagioclase component. The effectiveness of this process is difficult to gauge, however. Also, the more melt that is produced by contact fusion, the more difficult it becomes to preserve a high-pressure signature in the plagioclase composition. The mat becomes gravitationally unstable and ascends as diapirs of plagioclase and liquid with a few orthopyroxene megacrysts. Calculations of the size and time scale of development of gravitational instabilities by Longhi and Ashwal (1985) suggest reasonable thicknesses (~1 km) for the plagioclase-rich layers in the high-pressure chamber. Orthopyroxene megacrysts with intermediate Al_2O_3 (5–7 wt%) may represent reequilibration or continued crystallization during the early part of the ascent. At some point though, the orthopyroxene megacrysts must be isolated from the liquid, and this is relatively easy to envision in a mush or crystal-rich suspension. Intrusion as a crystal-liquid mixture also allows for deformation of the plagioclase to form bent twins such as those seen in parts of the Laramie (Longhi and Ashwal, 1985) and Nain (Wiebe, 1978) anorthosites. Since the plagioclase field expands with falling pressure (Fig. 7), the liquid becomes saturated only in plagioclase. Upon reaching the level of anorthosite emplacement (~3 kbar), the liquid crystallizes its excess plagioclase component and then additional plagioclase and mafic minerals in cotectic proportions. More liquid-rich portions of the mush can develop undeformed crystals and perhaps modal layering such as in parts of the Harp Lake (Emslie, 1980) and Nain Complexes (Wiebe, 1990). Replenishment of the high-pressure magma chamber at depth leads to production of new batches of the evolved cotectic magma, some of which intrudes upward and forms dikes and small intrusive bodies like those represented by HLCA.

Conclusions

Based on our experiments, we can draw some conclusions about the parental magmas of anorthosites and about the processes by which anorthosites form.

1. Plagioclase-melt partitioning is a strong function of pressure. For both HLCA and 500B, high pressures are required to crystallize the intermediate plagioclase of anorthosite plutons. This observation is consistent with transport of plagioclase crystals from deep crustal levels in the formation of anorthosite complexes.

2. The work on sample 500B, the anorthositic dike from the Nain Complex, indicates that it cannot be a dry liquid or simple plagioclase-liquid suspension. This conclusion is in accordance with prior phase equilibria studies reviewed by Longhi and Ashwal (1984), which show that extremely anorthositic liquids cannot be produced by crystallization of basalt or by reasonable degrees of melting of mantle or lower crust under the dry conditions indicated for anorthosite formation. In addition, the compositions of the phases produced in the 500B experiments do not match those in the anorthosite plutons. Thus 500B is not a good candidate for the parental magma for anorthosites.

3. The experiments on HLCA, the synthetic analogue of high-Al gabbros from the Harp Lake Complex, show that it can produce the mineral compositions observed in anorthosite complexes. In particular, orthopyroxenes formed at 5–11.5 kbar closely resemble the orthopyroxene megacrysts found in many anorthosite complexes, and plagioclase compositions are consistent with a large portion of the plagioclase crystallizing at high pressure followed by final solidification at low pressures. HLCA is multiply saturated with plagioclase and two pyroxenes on the liquidus at 11.5 kbar, which suggests that it could represent a magma crystallizing in a deep-crustal or upper-mantle chamber. Density considerations show that a model in which plagioclase accumulates by flotation in such a high-pressure magma chamber is viable. The anorthosite plutons are then produced by a second stage in the process involving emplacement of plagioclase-liquid mushes or suspensions at shallower levels. Plagioclase crystallization continues after emplacement because of expansion of the plagioclase liquidus field upon decompression of the magma.

Acknowledgments

We thank D. Walker, M.C. Johnson, and R.A. Wiebe for critical readings of the manuscript, and J.H. Berg and C. Simmons for helpful reviews. R.A. Wiebe provided starting material 500B. M.S.F. was supported by an NSF Graduate Fellowship and NSF grant EAR-8903410 (C.E. Lesher), and the research was funded by NASA grant NAG-9-329 (J.L.). This work was also done as part of the International Geological Correlation Programme, Project 290. Lamont-Doherty Geological Observatory Contribution no. 4902.

References cited

Agee, C.B., and Walker, D. (1988) Static compression and olivine flotation in ultrabasic silicate liquid. Journal of Geophysical Research, 93, 3437–3449.

Akella, J., and Kennedy, G.C. (1971) Melting of gold, silver, and copper—Proposal for a new high-pressure calibration scale. Journal of Geophysical Research, 76, 4969–4977.

Anderson, J.L. (1980) Mineral equilibria and crystallization conditions in the Late Proterozoic Wolf River Rapakivi Massif, Wisconsin. American Journal of Science, 280, 289–332.

Ashwal, L.D., and Seifert, K.E. (1980) Rare-earth element geochemistry of anorthosite and related rocks from the Adirondacks, New York, and other massif-type complexes. Geological Society of American Bulletin, part II, 91, 659–684.

Ashwal, L.D., and Wooden, J.L. (1983) Sr and Nd isotope geochronology, geologic history, and origin of the Adirondack Anorthosite. Geochimica et Cosmochimica Acta, 47, 1875–1885.

Ashwal, L.D., Wooden, J.L., and Emslie, R.F. (1986) Sr, Nd, and Pb isotopes in Proterozoic intrusives astride the Grenville Front in Labrador: Implications for crustal contamination and basement mapping. Geochimica et Cosmochimica Acta, 50, 2571–2585.

Berg, J.H. (1977) Regional geobarometry in the contact aureole of the anorthositic Nain Complex, Labrador. Journal of Petrology, 18, 399–430.

——— (1979) Physical constraints and tectonic setting of the Nain complex. Geological Association of Canada Abstracts, 4, 39.

Birch, F. (1966) Compressibility, elastic constants. Geological Society of America Memoir, 97, 97–174.

Bottinga, Y., and Weill, D.F. (1970) Densities of liquid silicate systems calculated from partial molar volumes of oxide components. American Journal of Science, 269, 169–182.

Bowen, N.L. (1917) The problem of the anorthosites. Journal of Geology, 25, 209–243.

Boyd, J.R., and England, J.L. (1960) Apparatus for phase-equilibrium measurements of pressures up to 50 kilobars and temperatures up to 1750 °C. Journal of Geophysical Research, 65, 741–748.

Bridgwater, D. (1967) Feldspathic inclusions in the Gardar igneous rocks of south Greenland and their relevance to the formation of major anorthosites in the Canadian shield. Canadian Journal of Earth Sciences, 4, 995–1014.

Buddington, A.F. (1939) Adirondack igneous rocks and their metamorphism. Geological Society of America Memoir, 7, 354 p.

Duchesne, J.C. (1990) Origin and evolution of monzonorites related to anorthosites. Schweizerische Mineralogische und Petrographische Mitteilungen, 70, 189–198.

Duchesne, J.C., Maquil, R., and Demaiffe, D. (1985) The Rogaland anorthosites: Facts and speculations. In A.C. Tobi and J.L.R. Touret, Eds., The deep Proterozoic crust in the North Atlantic provinces, p. 449–476. Reidel, Dordtrecht, the Netherlands.

Dymek, R.F., and Gromet, L.P. (1984) The nature and origin of orthopyroxene megacrysts from the St-Urbain Anorthosite Massif, Quebec. Canadian Mineralogist, 22, 297–326.

Emslie, R.F. (1970) Liquidus relations and subsolidus reactions in some plagioclase bearing systems. Carnegie Institution of Washington Year Book, 69, 148–155.

——— (1975) Pyroxene megacrysts from anorthositic rocks: New clues to the sources and evolution of the parent magmas. Canadian Mineralogist, 13, 138–145.

——— (1980) Geology and petrology of the Harp Lake Complex, central Labrador: An example of Elsonian magmatism. Geological Survey of Canada Bulletin, 293, 136 p.

——— (1985) Proterozoic anorthosite massifs. In A.C. Tobi and J.L.R. Touret, Eds., The deep Proterozoic crust in the North Atlantic provinces, p. 39–60. Reidel, Dordtrecht, the Netherlands.

Emslie, R.F., and Lindsley, D.H. (1968) Experiments bearing on the origin of anorthositic intrusions. Carnegie Institution of Washington Year Book, 67, 108–112.

Fuhrman, M.L., Frost, R.B., and Lindsley, D.H. (1988) Crystallization conditions of the Sybille Monzosyenite, Laramie Anorthosite Complex, Wyoming. Journal of Petrology, 29, 699–729.

Ghiorso, M.S. (1985) Chemical mass transfer in magmatic systems. Contributions to Mineralogy and Petrology, 90, 107–120.

Green, T.H. (1969a) Experimental fractional crystallization of quartz diorite and its application to the problem of anorthosite origin. In Y.W. Isachsen, Ed., Origin of anorthosite and related rocks, memoir 18, p. 23–29. New York, State Museum and Science Service, Albany, New York.

——— (1969b) High-pressure experimental studies on the origin of anorthosite. Canadian Journal of Earth Sciences, 6, 427–440.

Kolker, A., and Lindsley D.H. (1989) Geochemical evolution of the Maloin Ranch pluton, Laramie Anorthosite Complex, Wyoming: Petrology and mixing relations. American Mineralogist, 74, 307–324.

Lesher, C.E., and Walker, D. (1988) Cumulate maturation and melt migration in a temperature gradient. Journal of Geophysical Research, 93, 10295–10311.

Longhi, J. (1991). Comparative liquidus equilibria of hypersthene normative basalts at low pressure. American Mineralogist, 76, 785–800.

Longhi, J., and Ashwal, L.D. (1984) A two-stage model for lunar anorthosites: An alternative to the magma ocean hypothesis. Lunar and Planetary Science, vol. 15, p. 491–492. The Lunar and Planetary Science Institute, Houston.

——— (1985) Two-stage models for lunar and terrestrial anorthosites: Petrogenesis without a magma ocean. Proceedings of the 15th Lunar and Planetary Science Conference, part 2. Journal of Geophysical Research, 90 (suppl.), C571–C584.

Longhi, J., and Pan, V. (1988) A reconnaissance study of phase boundaries in low-alkali basaltic liquids. Journal of Petrology, 29, 115–148.

Miller, J.D., Jr., and Weiblen, P.W. (1990) Anorthositic rocks of the Duluth Complex: Examples of rocks formed from plagioclase crystal mush. Journal of Petrology, 31, 295–339.

Mo, X., Carmichael, I.S.E., Rivers, M., and Stebbins, J. (1982) The partial molar volume of Fe_2O_3 in multicomponent silicate liquids and the pressure dependence of oxygen fugacity in magmas. Mineralogical Magazine, 45, 237–245.

Morse, S.A. (1975) Plagioclase lamellae in hypersthene: Tikkoatokhakh Bay, Labrador. Earth and Planetary Science Letters, 26, 311–336.

——— (1982) A partisan review of Proterozoic anorthosites. American Mineralogist, 67, 1087–1100.

Phinney, W.C., Morrison, D.A., and Maczuga, D.E. (1988) Anorthosites and related megacrystic units in the evolution of Archean crust. Journal of Petrology, 29, 1283–1323.

Ranson, W.A. (1986) Complex exsolution in inverted pigeonite: Exsolution mechanisms and temperatures of crystallization and exsolution. American Mineralogist, 71, 1322–1336.

Simmons, E.C., and Hanson, G.N. (1978) Geochemistry and origin of massif-type anorthosites. Contributions to Mineralogy and Petrology, 66, 119–135.

Skinner, B.J. (1966) Thermal expansion. Geological Society of America Memoir, 97, 75–96.

Walker, D., and Agee, C.B. (1987) Ureilite compaction. Meteoritics, 23, 81–91.

Weaver, J.S., and Langmuir, C.H. (1990) Calculation of phase equilibrium in mineral-melt systems. Computers and Geosciences, 16, 1–19.

Wiebe, R.A. (1978) Anorthosite and associated plutons, southern Nain Complex, Labrador. Canadian Journal of Earth Sciences, 15, 1326–1340.

——— (1979) Anorthositic dikes, southern Nain Complex, Labrador. American Journal of Science, 279, 394–410.

——— (1980) Anorthositic magmas and the origin of Proterozoic anorthosite massifs. Nature, 286, 564–567.

——— (1986) Lower crustal cumulate nodules in Proterozoic dikes of the Nain Complex: Evidence for the origin of Proterozoic anorthosites. Journal of Petrology, 27, 1253–1275.

——— (1990) Evidence for unusually feldspathic liquids in the Nain Complex, Labrador. American Mineralogist, 75, 1–12.

Yoder, H.S., and Tilley, C.E. (1962) Origin of basalt magmas: An experimental study of natural and synthetic rock systems. Journal of Petrology, 3, 342–532.

Manuscript received March 25, 1991
Manuscript accepted January 6, 1992